



## Article (refereed) - postprint

---

Robinson, David A.; Abdu, Hiruy; Lebron, Inma; Jones, Scott B. 2012 Imaging of hill-slope soil moisture wetting patterns in a semi-arid oak savanna catchment using time-lapse electromagnetic induction.

Crown Copyright © 2011 Published by Elsevier B.V.

This version available <http://nora.nerc.ac.uk/16558/>

NERC has developed NORA to enable users to access research outputs wholly or partially funded by NERC. Copyright and other rights for material on this site are retained by the rights owners. Users should read the terms and conditions of use of this material at <http://nora.nerc.ac.uk/policies.html#access>

NOTICE: this is the author's version of a work that was accepted for publication in . *Journal of Hydrology*. Changes resulting from the publishing process, such as peer review, editing, corrections, structural formatting, and other quality control mechanisms may not be reflected in this document. Changes may have been made to this work since it was submitted for publication. A definitive version was subsequently published in . *Journal of Hydrology*, 416-417. 39-49. [10.1016/j.jhydrol.2011.11.034](https://doi.org/10.1016/j.jhydrol.2011.11.034)

[www.elsevier.com/](http://www.elsevier.com/)

Contact CEH NORA team at  
[noraceh@ceh.ac.uk](mailto:noraceh@ceh.ac.uk)

The NERC and CEH trademarks and logos ('the Trademarks') are registered trademarks of NERC in the UK and other countries, and may not be used without the prior written consent of the Trademark owner.

Elsevier Editorial System(tm) for Journal of Hydrology  
Manuscript Draft

Manuscript Number:

Title: Imaging of hill-slope soil moisture wetting patterns in a semi-arid oak savanna catchment using time-lapse electromagnetic induction

Article Type: Research Paper

Keywords: Soil science, induction, EMI, water content, hydrogeophysics, time domain reflectometry

Corresponding Author: Dr. David Robinson,

Corresponding Author's Institution:

First Author: David A Robinson

Order of Authors: David A Robinson; David Robinson; Hiruy Abdu; Inma Lebron

Suggested Reviewers: Jan MH Hendrickx  
Prof, Dept of Earth & Environmental Science , New Mexico Tech  
hendrick@nmt.edu  
Broad experience in EMI, soils and hydrology

Cristine LS Morgan  
Ass Prof, Texas A&M  
cmorgan@ag.tamu.edu  
Broad experience in EMI, soils and hydrology

James Doolittle  
Research Soil Scientist, USDA  
jim.doolittle@lin.usda.gov  
Extensive experience with EMI and soils, some hydrology

Andrew Western  
Assoc. Prof, Department of Civil and Environmental Engineering, University of Melbourne  
a.western@unimelb.edu.au  
Strong experience in soil moisture spatial patterns in hydrology

Jon Wraith  
Dean, University of New Hampshire  
jon.Wraith@unh.edu  
Strong experience with soils, spatial water content determination using TDR

1 **Imaging of hill-slope soil moisture wetting patterns in a semi-arid oak savanna**  
2 **catchment using time-lapse electromagnetic induction**

3

4

5

David A. Robinson <sup>a#, c</sup>

6

Hiruy Abdu <sup>b</sup>

7

Inma Lebron <sup>a#, c</sup>

8

Scott B. Jones <sup>b</sup>

9

10 a# Now at: Center for Ecology and Hydrology, Environment Centre Wales, Deiniol Road,

11

Bangor, Gwynedd, UK

12

b Dept of plants, soils and climate, Utah State University, Logan, UT.

13

c Dept of Geophysics, Stanford University, Stanford, CA.

14

15

16 \* To whom correspondence should be addressed. E-mail: [darearthscience@yahoo.com](mailto:darearthscience@yahoo.com)

17

18 Key Words: Soil science, induction, EMI, water content, hydrogeophysics, time domain  
19 reflectometry

20

21

22 Abbreviations: EMI Electromagnetic induction, EC<sub>a</sub> Bulk soil electrical conductivity, GPR

23

Ground penetrating radar, sGs Sequential Gaussian simulation, TDR Time domain reflectometry,

24

VWC Volumetric water content.

1  
2  
3  
4  
5  
6  
7  
8  
9  
10  
11  
12  
13  
14  
15  
16  
17  
18  
19  
20  
21  
22

**Abstract**

Soil moisture is a fundamental hydrological state variable and its spatial pattern is important for understanding hydrological processes. Determination of catchment-scale soil moisture status and distribution at intermediate scales (0.1-1 km<sup>2</sup>) is challenging. Primarily because multi-point measurements using sensors are often impractical, while remote sensing resolution is often too coarse. Geophysical methods, e.g. electromagnetic induction (EMI), offer potential for bridging this gap. Our objective was to test the use of time-lapse EMI surveys to separate the influences of ‘static’ soil variables, e.g. texture, from ‘dynamic’, e.g. soil moisture. A novel differencing approach is proposed for estimating soil moisture, subtracting the electrical conductivity (EC<sub>a</sub>) of the driest seasonal soil map from the EC<sub>a</sub> collected during subsequent wetting. By doing this, and comparing results with TDR determined soil moisture, we improve the correlation from  $r^2 = 0.28$  to  $r^2 = 0.48$ . EC<sub>a</sub> measurements are observed to be correlated in time ( $r^2 > 0.7$ ), but fall into two distinct groups, corresponding to times before and after the onset of stream flow, supporting the concept of preferred soil moisture states. Catchment wetness index predicts areas of convergence resulting in overland flow and stream flow. However, the spatial pattern of soil moisture does not mirror the wetness index, as others have found. We contend that the use of time-lapse imaging provides important insight into the distribution and dynamics of catchment-scale soil moisture, but acknowledge its limitations of requiring moisture dependent contrast of EC<sub>a</sub>, which will not occur in some soils.

## 1 **Introduction**

2

3         Soil moisture controls the structure, function and diversity of vegetation (Rodriguez-  
4 Iturbe et al., 1999); it also controls the partitioning of precipitation between infiltration and  
5 runoff which in turn affects stream flow and soil erosion (Loague, 1992). There remains distinct  
6 interest in hydrology to be able to determine antecedent catchment scale soil moisture to help  
7 calibrate rainfall-runoff simulations, (e.g. Stephenson and Freeze, 1974; Wilson et al., 2005). At  
8 the sample scale the soil moisture influences both soil physical behavior, such as mechanical  
9 strength, temperature and oxygen levels, and soil biogeochemical behavior, by exerting control  
10 over microbial activity, which controls processes such as respiration, CO<sub>2</sub> efflux, and  
11 nitrification (Schjonning et al., 2003). Patterns of soil moisture are intimately linked with the  
12 distribution of soil types and vegetation, and in turn with the landscape and topography (Wilson  
13 et al., 2005; Lin et al., 2006). Recent interest and advances in describing soil moisture have  
14 resulted in a number of recent reviews on different aspects including ecohydrology (Rodriguez-  
15 Iturbe et al., 1999), climate (Seneviratne et al., 2010), vadose zone hydrology (Vereecken et al.,  
16 2008), scaling (Western et al., 2002) and measurement (Robinson et al., 2008a). Much of this  
17 literature, synthesized, points to an intermediate scale measurement gap which impedes a fuller  
18 understanding of catchment processes. Due to this lack of reliable soil moisture data; Western et  
19 al. (1999) stated, “*Point values are notoriously poor in identifying spatial organization.*  
20 Williams (1988) and Schmutge and Jackson (1996), among others, point out that “*the apparent*  
21 *randomness sometimes observed for hydrologic variables is largely a consequence of using point*  
22 *measurements. What is needed are high-resolution observations of soil moisture patterns based*  
23 *on a large number of point samples.*”

24         Determining moisture patterns and response at catchment scales (0.1-1 km<sup>2</sup>) is a major  
25 measurement challenge, that is often too large for point-measurement using sensors such as time  
26 domain reflectometry (TDR) (Robinson et al., 2003), but too small for discrimination using  
27 remote sensing (Engman, 1995). At small scales (<10 ha) point sensors such as TDR have been  
28 used to determine spatial patterns of soil moisture (Wraith et al., 2005; Western and Grayson,  
29 1998), however measurements can be time consuming and impractical, in hard or stony soils, or  
30 as the spatial scale increases. In addition, small support volumes (Ferré et al., 1998) tend to make  
31 measurements less appealing for catchment application; we contend that many point sensors

1 capture too small a sample volume of moisture measurement to be most pertinent to catchment  
2 scale hydrology. Remote sensing is often used at the sub-watershed scale (1–80 km<sup>2</sup>), but the  
3 resolution is too coarse for catchment scale, is surface constrained (~0-5cm) when moist, and  
4 often impractical in complex undulating terrain with a dense canopy. Obtaining accurate  
5 catchment scale soil moisture spatial estimates or at least changes in soil moisture, with  
6 sufficient temporal resolution remains both a logistical and measurement challenge (Robinson et  
7 al., 2008a).

8         Alternative approaches to bridging this divide have been proposed, one is to use networks  
9 of sensors offering high temporal resolution with reasonable spatial coverage (Cardell-Oliver et  
10 al., 2005; Bogena et al., 2007), while another is to utilize non-invasive geophysical methods  
11 (Rubin and Hubbard, 2006). Geophysical methods have been used extensively for groundwater  
12 investigation (Dobecki and Romig, 1985), but a suite of electromagnetic methods offer real  
13 opportunity for advancing the hydrological understanding at the watershed scale (Robinson et al.,  
14 2008b). Ground penetrating radar GPR, has been tested and applied successfully at the field /  
15 catchment scale (Huisman et al., 2003). However, GPR has limitations, not working well in clay  
16 or electrically conductive soils, contact issues in dense shrub, as well as requiring more  
17 sophisticated data interpretation. Electromagnetic induction (EMI), is an alternative non-invasive  
18 technique which measures bulk soil electrical conductivity (EC<sub>a</sub>) (Hendrickx and Kachanoski,  
19 2002), with a large support volume (~1 m<sup>3</sup>) making it particularly attractive for catchment scale  
20 studies. Although non-invasive geophysical methods are relatively fast for mobile measurements,  
21 all geophysical methods tend to require more extensive calibration than point sensors, either  
22 because of changing support volumes, or because they measure properties that are also  
23 influenced by other environmental variables.

24         At small scales, e.g. 1D profiles, dielectric measurements such as TDR are favored over  
25 electrical conductivity measurements because they are less sensitive to texture and temperature  
26 (Friedman, 2005; Robinson et al., 2003). However, the ability of electrical measurements to  
27 capture high temporal and spatial resolution, 2-D profiles, (Michot et al., 2003, Samouelian et  
28 al., 2005) with minimum soil invasion has renewed interest in their application to hydrology.  
29 Recently researchers have begun to consider EMI's utility for determining water content, and  
30 determining soil and hill-slope hydrological processes (Kachanoski and de Jong, 1988; Sheets  
31 and Hendrickx, 1995; Sherlock and McDonnell, 2003; Huth and Poulton, 2007; Robinson et al.,

1 2008c; Abdu et al., 2008; Tromp-van Meerveld and McDonnell, 2009; Robinson et al., 2009). A  
2 firm understanding of soil properties affecting electromagnetic field behavior is helpful in  
3 understanding when EMI can be applied, as it is not suitable for all circumstances. We have  
4 shown previously that EMI surveys are of use in imaging catchment scale soil textural spatial  
5 patterns where the salinity of the soil solution extract electrical conductivity, ( $EC_e$ ) is not a major  
6 contributor to the  $EC_a$  (Abdu et al, 2008). In order to map texture, an electrical contrast is  
7 required with differing particle size. EMI responds to the quantity of ions in the soil, so clays that  
8 adsorb more ions on their surfaces, and have higher surface areas, compared to sands and silts  
9 give greater responses. This is exploited to determine texture, but it is determined by the clay  
10 mineralogy; soil with 2:1 smectite or illite clays tend to contrast well with silica sands, but 1:1  
11 kaolinites in general do not, given their low ion adsorption.

12 EMI measurements combine sufficient spacing, extent and support (i.e. scale triplet,  
13 Blöschl and Grayson, 2000) to capture the small and large scale variability of soil properties  
14 across catchments. EMI-based  $EC_a$  measurements have been used by researchers attempting to  
15 infer different soil properties, soil  $EC_a$  is related to texture, moisture, soil water electrical  
16 conductivity ( $EC_w$ ), soil depth and temperature (Friedman, 2005) and has often been used in soil  
17 mapping by correlating signal response with soil variables of interest (Hendrickx and  
18 Kachanoski, 2002; Corwin and Lesch. 2003; Lesch et al., 2005). Although the measurement  
19 response varies with other variables, it does no-more-so than other landscape scale measurement  
20 techniques used for determining moisture such as, active microwave remote sensing which  
21 depends on dielectric contrast, surface roughness, layering, vegetation, soil wetness dependent  
22 support volume, temperature, and salinity etc. Careful measurement application with EMI can be  
23 used to maximize the response of some variables and minimize others. Determining the best  
24 ways to do this is an important area of EMI research. Some of the more tested applications  
25 include: soil salinity estimation (Lesch et al., 2005), estimating claypan depth (Doolittle et al.,  
26 1994); inferring topsoil depth in claypan soils (Sudduth et al., 2001); producing field scale  
27 (Triantafilis and Lesch, 2005), and regional scale (Harvey and Morgan, 2009) textural maps, and  
28 delineation of soil classification zones (Vitharana et al., 2008). All these applications to obtain  
29 'static' properties tend to utilize single EMI response surfaces, snapshots of  $EC_a$ . However,  
30 researchers have begun to exploit time-lapse imaging where consecutive collection the soil  $EC_a$   
31 response at different times in the same location can start to be used to differentiate between the

1 contributions of the constant or ‘static’ components of the soil, like particle size distribution,  
2 from the more dynamic ones like wetting patterns (Robinson et al., 2009; Besson et al., 2010).  
3 Despite the utility of EMI data for visualizing soil spatial variability, time-lapse imaging offers  
4 the potential to go beyond pattern recognition to obtain quantitative estimates of soil moisture  
5 change.

6 Therefore, the objectives of this research were to 1) identify soil spatial variability and  
7 wetting patterns in a catchment by collecting time-lapse EMI data, 2) to estimate catchment  
8 textural patterns, as related to soil hygroscopic water, by analyzing wet and dry EC<sub>a</sub> response and  
9 infer optimal correlation, and 3) to use an electrical model to determine moisture content from  
10 direct estimation using TDR, and contrast this with a novel time-lapse differencing calibration  
11 approach.

12

## 13 **Materials and methods**

14

### 15 *Field site*

16 Our field site was located on the Stanford University Foothills, academic reserve, which  
17 serves as a protected Mediterranean type ecological area at the base of the Santa Cruz  
18 Mountains. The reserve is a mixed oak-grass savanna on rolling hills between 60 and 140 m in  
19 elevation. Up until the 1980's the location had been grazed by cattle for the previous 50 yrs.  
20 Research indicated that the age distribution of the trees was highly skewed, and that only a small  
21 number of seedlings were surviving past their 10th year (Zebroski and McBride, 1983). By the  
22 end of the 1980's approximately half the reserve had been closed to cattle grazing including our  
23 study area. We chose an area largely unaffected by anthropogenic activity since the cessation of  
24 grazing. The woodland on the reserve is dominated by oak, including the evergreen coast live  
25 oak (*Quercus agrifolia*), the deciduous valley oak (*Quercus lobata*) and blue oak (*Quercus*  
26 *douglasii*) with some California buckeye (*Aesculus californica*). The savanna is located on soil  
27 types loosely classified as loams, clays and stony clays (Schwan et al., 1997).

28 Our field site was towards the SE corner of the reserve, in a small catchment ~ 4ha  
29 (Figure 1). The catchment drops from ~120 m at its highest elevation point to 76 m where it joins  
30 with another small catchment. The site is appealing from the soils perspective as the parent  
31 material splits the site roughly in half, with the upper portion of the catchment on basalt (Tpm,

1 Page Mill Basalt), and the mid to lower portion of the catchments being on  
2 sedimentary/sandstone formations (Tw, Whiskey Hill Formation; QTsc, Santa Clara Formation;  
3 Tlad, Ladera Sandstone) (Brabb et al., 2000); this results in a gradation of texture from the top of  
4 the catchment to the bottom from clay to sandy loam. No formal soil survey has been conducted  
5 on this site. However, soils were sampled and soil hygroscopic water content determined in  
6 combination with texture-by-feel. These analyses indicated the upper portion of the catchment  
7 was dominated by clay and clay loams, grading into sandy loams on the sandstone spurs, and  
8 transitioning to loams in the lower portion of the catchment, where erosion and deposition has  
9 mixed the two materials. In addition, we also mapped the location of rock outcrops using the  
10 GPS which serve to better define the location of the boundary between the basalt and the  
11 sandstone and hence the soil type boundary.

12 The climate of this area is Mediterranean with hot dry summers and cool wet winters  
13 with 40 cm average annual rainfall, the majority of which falls between September and April and  
14 a potential evaporation of 120 cm. Weather data was obtained from a nearby weather station,  
15 located at the Jasper Ridge reserve. Rainfall patterns during the study were typical for this area,  
16 with a dry summer followed by precipitation events increasing in frequency and intensity as the  
17 fall progressed into the winter.

18

### 19 *EMI equipment and measurement*

20 In non-saline soils the EMI signal is related to texture, moisture, solution electrical  
21 conductivity ( $EC_e$ ) and soil depth (Friedman, 2005). In non-saline soils we can assume that the  
22 moisture is the dynamic phase, changing with precipitation and evaporation, whereas the other  
23 properties are essentially 'static'. By adopting a time-lapse imaging approach we can try to tease  
24 apart the 'static' and 'dynamic' properties of the soil.

25 EMI sensors are ideally suited to obtaining measurements in rugged terrain (Abdu et al.,  
26 2008). The instrument measures non-invasively while suspended over the soil (McNeill, 1980).  
27 The 1.4 m long instrument has a transmitter coil at one end and a receiver coil at the other end.  
28 Magnetic field loops are generated by the transmitter and penetrate into the soil to a depth  
29 determined by the coil spacing (Callegary et al., 2007). We used a Dualem 1-S (Dualem.com,  
30 Milton, ON, Canada) with the coils approximately 1 m apart. This means that 70% of the signal  
31 response will be integrated over a depth of 1.5 m for the coils in the vertical orientation and 0.5

1 m for the coils in the horizontal orientation (Abdu et al., 2007), giving the instrument a sensing  
2 depth equivalent to a pedon in terms of scale. Callegary et al. (2007) have shown that in soils  
3 with conductivity that range up to  $100 \text{ mS m}^{-1}$  the depth of exploration (DOE) is attenuated to  
4 less than 1 m, vertically, and is perhaps 40 cm for the horizontal orientation. The horizontal  
5 orientation is strongly weighted to the surface and we used this data in our research. The primary  
6 magnetic field creates current loops in the soil, which in turn induce a secondary magnetic field.  
7 The receiver coil measures both the primary and secondary magnetic fields. Therefore the  $\text{EC}_a$   
8 can be determined from the ratio of the primary and secondary magnetic fields under the  
9 assumption of low-induction numbers (McNeill, 1980). The Dualem 1-S is preferred for this  
10 style of work as it doesn't require manual calibration and is sensitive to low bulk electrical  
11 conductivity soils (Abdu et al., 2007).

12 The Dualem-1S was used to collect geo-referenced soil  $\text{EC}_a$  measurements non-  
13 invasively over a 6 month period between Sept 2007 and February 2008. The georeferenced  $\text{EC}_a$   
14 data was acquired using a handheld geographic information system (HGIS, StarPal Inc., Fort  
15 Collins, CO) program installed on an Allegro handheld field computer (Juniper Systems, Logan,  
16 UT). The field computer interfaced with the Dualem and a GPS with the HGIS software  
17 managing the data acquisition of position and  $\text{EC}_a$  measurement. The GPS used was a Holux  
18 GPSlim 240 (Holux Technology Inc., Hsinchu, Taiwan) with a Sirf III chip set. The advantage of  
19 this type of GPS is the sensitivity, designed for urban canyons; the GPS operates well under tree  
20 canopies, enabling spatial measurement in these savanna ecosystems. GPS data was collected in  
21 Latitude and Longitude format using the WGS84 reference, which were later converted to UTM  
22 coordinates using spreadsheet software (Dutch, 2010).

23 We conducted 9 surveys across a 4 ha field site, over a period of six months, during  
24 which time we followed the catchments wetting after the dry Mediterranean summer. EMI  
25 survey was conducted by traversing the catchment following a contouring pattern; each survey  
26 collected about 4000 measurement points over several hours. Surveys were carried out over a  
27 range of soil water contents completely dry following summer, to soil saturation and the  
28 presence of overland flow. The instrument was carried at a height of approximately 10 cm above  
29 the ground surface during mapping.

30  
31

1 *TDR equipment and measurement*

2 TDR has become a standard method for the measurement of soil moisture. The TDR  
3 technique (Robinson et al., 2003) was used in a mobile configuration using a Campbell TDR 100  
4 (Campbell Scientific Inc., Logan, UT). The TDR device was connected to a data logger and  
5 measurement controlled by a switch, in addition a handheld GPS with Sirf III chipset was used to  
6 collect location data for each measurement. The TDR probe used for measurement had 3 rods  
7 and was 15 cm long. It was mounted on a handle, like that of a spade, so it could be routinely  
8 inserted into the ground vertically. A practical consideration for the use of TDR in the mobile  
9 mode is the soil hardness. In dry or rocky soils measurements are not feasible for routine data  
10 collection. We found that following the dry summer the soils were too hard for routine TDR  
11 probe insertion. We had to wait until the soil wetted thoroughly, in January/February before we  
12 could make measurements. This is a real limitation for the use of handheld TDR or other  
13 insertion sensors in hard soils. Measurements were made on Feb 28, 2008 following the  
14 measurement path of the EMI survey carried out at the same time. Ninety TDR measurements  
15 were collected in the time span of about four hours, about twice the time for the EMI surveys  
16 (Figure 1). Water content was estimated using the standard Topp et al., (1980) calibration  
17 equation and  $EC_a$  was determined following calibration of the probe in solutions.

18

19 *Soil sampling*

20 TDR estimates water content directly from the dielectric measurement, where as  $EC_a$   
21 estimation of water content requires knowledge of the soil porosity and solution electrical  
22 conductivity. We estimated the areal mean  $EC_e$  and porosity from a set of soil measurements  
23 from across the catchment. We adopted a random sampling design and collected 64 soil samples  
24 which were analyzed for solution  $EC_w$  using a 2:1 dilution,  $EC_e$  was estimated from this by  
25 multiplying the result by 3.25 which is interpolated from dilutions (Landon, 1991). Bulk density  
26 was measured to 20 cm using a standard volumetric auger method, with the soil samples dried at  
27 105 °C to determine the solid mass (Gee and Bauder, 1986). We also used these samples to  
28 determine the hygroscopic water content at 50% relative humidity as an indicator of clay content  
29 spatial distribution.

30

31 *Ground conductivity modeling and geostatistics*

1           Electrical conductivity measurements applied to the determination of  $EC_a$  are reviewed in  
2 (Freeland, 1989). The ability of electrical geophysical methods to collect spatial data, such as DC  
3 resistivity and electromagnetic induction (EMI) that are minimally- or non-invasive, are leading  
4 to renewed interest in determining VWC using electrical conductivity. An important aspect of  
5 moisture retrieval from electrical methods is the need for calibration. A number of models have  
6 been presented to determine the bulk soil electrical conductivity as a function of soil parameters.  
7 Empirical models include those based on  $EC_a$  measurements in rock (Archie, 1942) and those  
8 produced for saline soils (Rhoades et al., 1989). A more physically based approach was proposed  
9 by Mualem and Friedman, (1991) which was based on the water release characteristics of the  
10 soil. This resulted in a simple model requiring the  $EC_w$ , moisture content and porosity to estimate  
11 the  $EC_a$ . Given the small number of parameters required to determine  $EC_a$ , and conversely  
12 retrieve soil moisture we adopted this model for the interpretation of our data. The model can be  
13 simplified to:

14

$$15 \quad EC_a = EC_w \theta_{sat}^{1.5} (\theta / \theta_{sat})^{2.5} \quad (1)$$

16

17 where  $\theta_{sat}$  is the saturated water content. This model reduces to  $\theta_{sat}$  being raised to an exponent of  
18 1.5 for saturated soil. Equation (1) was found to describe  $EC_a$  in a wide range of coarse and  
19 stable structured soils. Adding the influence of surface conductivity  $EC_s$ , various authors  
20 (Friedman, 2005; Nadler, 2005) have suggested a general formulation of Archie's law (Archie,  
21 1942) which can be extended to unsaturated soil (Telford et al., 1990), however we chose not to  
22 follow this line because there is little information on the expected values for surface  
23 conductivity, and this essentially adds further fitting parameters to the modeling.

24           A novel aspect to our approach of applying the  $EC_a$  model was to use a differencing  
25 method to obtain  $EC_a$  values on which to apply the model. Soil texture variability will add a  
26 'surface' conductivity component to the data to varying degrees as soil texture alters around the  
27 catchment. Rather than try to estimate this through collecting texture samples, we made an  
28 assumption that this textural variation and surface conductivity contribution could be minimized  
29 by assuming that this was equivalent to  $EC_a$  in dry soil. In order to estimate the water content we  
30 therefore subtracted the interpolated measurements for the Sept 28 mapping from all other  $EC_a$   
31 response surfaces collected subsequently. These differenced  $EC_a$  values were then used in

1 Equation 1 to estimate water content. We evaluated the results of doing this by comparing data  
2 that was differenced and data that was not with TDR estimates of water content for Feb 28, 2008.

3 Quality assurance and quality control (QA/QC) procedures were applied to the EMI data  
4 collected. The  $EC_a$  measurements were downloaded to a spreadsheet and checked for quality. In  
5 the spreadsheet the data can be plotted as a time-series to identify  $EC_a$  outliers, and to remove  
6 multiple data collected at the same location while the surveyor took a break. Some outliers were  
7 identified, which were associated with metallic litter that had found its way into the catchment.  
8 By examining the GPS speed any extra measurements can be removed from the data when the  
9 mapper was stationary.

10 Following these QA/QC procedures the data was analyzed using geostatistics to perform  
11 interpolation, and simulation of uncertainty. The  $EC_a$  data collected was mostly skewed giving a  
12 lognormal appearance which is common for soils. In order to meet the underlying assumptions of  
13 kriging, that the data have a Gaussian distribution, all data were normal score transformed (NS)  
14 during analysis using SGEMS (Remy et al., 2009). More comprehensive treatment of the  
15 geostatistics can be found in Goovaerts (1997), we provide a summary of the multi-gaussian  
16 procedure here. The NS data were fitted with a semivariogram, and kriged using simple kriging  
17 on a 2m grid. Once kriged, the data were back-transformed to produce a final interpolated  $EC_a$   
18 response surface of the catchment.

19 Sequential Gaussian Simulation (sGs) was used to determine the spatial uncertainty of the  
20 data collected on Feb 28, 2008. In any prediction process, quantifying the uncertainty of the  
21 estimate is helpful for the comparison of the data collection methods. Kriging, which gives the  
22 minimum local error variance in the generalized least squares sense, is affected by a smoothing  
23 of the local variance of the attribute being predicted. Conditional simulation or stochastic  
24 imaging generates equally probable realizations of the property being studied in order to better  
25 quantify the uncertainty of the property at unsampled locations. Simulation focuses on honoring  
26 the data values while replicating the global statistics of the data distribution and the variogram  
27 model (Goovaerts, 1999). A more commonly used approach in environmental science  
28 applications is to predict the spatial uncertainty using sequential Gaussian simulation. We used  
29 the algorithms available in SGEMS to obtain the e-type mean and conditional variance from 100  
30 simulations. The e-type mean can be compared with the interpolated  $EC_a$  or TDR measurement  
31 values obtained from kriging.

1 Statistical analysis of nine kriged EC<sub>a</sub> maps were conducted using correlation analysis  
 2 and temporal or rank stability procedure described by Vachaud et al. (1985), to compare all the  
 3 data, the dry (sept 27, Oct 4, Oct 22) and the wet (Jan 6, Jan 10, Feb 22) with the hygroscopic  
 4 water content data. In this procedure the difference  $\Delta_{ij}$  of each individual observation  $S_{ij}$  to the  
 5 average  $\bar{S}_j$  for the respective sampling time  $j$  is calculated with:

$$6 \quad \Delta_{ij} = S_{ij} - \bar{S}_j \quad (2)$$

7 And the relative difference is calculated by:

$$8 \quad \delta_{ij} = \frac{\Delta_{ij}}{\bar{S}_j} \quad (3)$$

9 For each sampling location an average relative difference  $\bar{\delta}_{ij}$  is calculated by:

$$10 \quad \bar{\delta}_{ij} = \frac{\sum_{j=1}^9 \delta_{ij}}{9} \quad (4)$$

11 for the nine sampling campaigns as well as its standard deviation  $\sigma$ . The resulting values were  
 12 added to the mean of the average EC<sub>a</sub> values for each mapping to provide a list of EC<sub>a</sub> values  
 13 that could be compared against the hygroscopic water values.

14 Catchment topography was determined by using the altitude measured using the GPS  
 15 receiver. Five of the surveys, with consistent data, were chosen for analysis. Each dataset was  
 16 interpolated using the normal score/ simple kriging approach described. The average altitude was  
 17 determined for each data set; four of the data sets were then corrected to the data set with the  
 18 middle ranked altitude by adding or subtracting the difference between averages. The average  
 19 altitude was 98.2 m and the average standard deviation was 3.3 m; the range was 5.8 m. After  
 20 correction to the mean the average standard deviation was reduced to 2.4 m between the data  
 21 sets, with a maximum and minimum altitude of 125 and 67 m respectively.

22

### 23 *Soil wetness index*

24 In modeling approaches, the spatial distribution of soil moisture is often assumed to  
 25 mirror that of a terrain attribute such as the wetness index (Kirkby, 1975; Beven and Kirkby,  
 26 1979; Grayson and Western 2001). Pursuant to this a number of soil wetness indices were  
 27 proposed for predicting the spatial distribution of zones of soil moisture (O' Loughlin, 1986;

1 Quinn et al., 1995; Barling et al., 2004). The wetness index represents the propensity of any  
2 point in the catchment to develop saturated conditions (Beven, 2001):

$$3 \quad \text{wetness index} = [\ln(a/\tan(\beta))] \quad (5)$$

4  
5  
6 where  $a$  = the upslope area, per unit contour length, contributing flow to a pixel;  $\tan \beta$  = the  
7 local surface slope angle acting on a cell (taken to approximate the local hydraulic gradient under  
8 steady-state conditions). Wetness index can be determined using the DTA-ANALYSIS software  
9 described in (Beven, 2001). Pits and sinks are identified in the elevation matrix, sinks can be  
10 removed using the Automatic-Sink-Removal tool, which uses successive averaging of  
11 surrounding elevations to resolve pits.

## 12 13 **Results and discussion**

14  
15 Precipitation data, EMI mapping times and all the EMI  $EC_a$  response surfaces are  
16 presented in Figure 2. The first light rainfall fell in September (Fig. 2A), a few days before the  
17 first EMI data collection, but the water quickly evaporated. By this stage in the year the clay soil  
18 was so dry that removal from the field to the laboratory actually increased the water content  
19 through the adsorption of hygroscopic water from the more humid laboratory atmosphere.  
20 Rainfall events increased in magnitude and frequency during the fall, but it wasn't until late  
21 December that the more significant storm events occurred. The first stream-flow was observed in  
22 the catchment after the rainfall on January 4<sup>th</sup> and 5<sup>th</sup>. Flow was then maintained, and continued  
23 until after the final mapping at the end of February 2008. The soil  $EC_a$  response surfaces (Fig.  
24 2B) correspond to dates indicated by the green lines on Figure 2A. Mapping in September and  
25 early October showed the least distinctive pattern, but a rainfall event in mid October (~10 mm)  
26 wetted the soil enough to see the emergence of distinct outlines following flow-paths and  
27 consistent with convergence zones; these became more pronounced with time and increasing  
28 wetting. The dominance of the clay soil in the upper portion of the catchment is indicated by the  
29 red, high  $EC_a$  values; note the jump in scale after the January rainfall which satiated the soil and  
30 resulted in stream-flow generation. Figure 2C shows the histograms for the  $EC_a$  data and a  
31 distinctive shift from left skewed to a bimodal distribution, between lines 6 and 7 (Fig. 2C); that

1 occurs at the beginning of January, consistent with the large storm event. Bimodal peaks are  
2 observable in all the histograms apart from the first two in September and early October. The  
3 bimodal peaks gradually move apart until early January, when they completely separate into two  
4 distinct distributions. The transition at the beginning of January is also marked by the reduction  
5 in correlation between the  $EC_a$  response surfaces before the January wetting and after (Table 1).  
6 Table 1 indicates that  $EC_a$  response surfaces prior to January 6<sup>th</sup> show reasonably good  
7 correlation with each other with  $r^2$  values  $\sim 0.7$ . Correlation increases after January 1<sup>st</sup> between  
8 the response surfaces to  $>0.9$ . The correlation between the wet response surfaces collected after  
9 January 1<sup>st</sup> and the response surfaces for September and October is poor, indicating a distinct  
10 change in spatial pattern. The wetting event in early January appears to mark a threshold in  
11 wetting where the hydrological response of the catchment changes abruptly and stream flow  
12 appears. It was observed that once streamflow was initiated it was maintained until after the end  
13 of observations on Feb 28<sup>th</sup>. The change in the  $EC_a$  patterns results in changes in the range of the  
14 semi-variograms (Figure 2D). In September the range was 72 m, which increased to 132 m by  
15 January 1<sup>st</sup>, and then 134, 157, and 115 m for the subsequent January 6<sup>th</sup>, 10<sup>th</sup> and February 28<sup>th</sup>  
16 measurements. This increase in the range of the autocorrelation is consistent with the emergence  
17 of the distinctive  $EC_a$  patterns on the ground.

18 Interpolated measurements of hygroscopic water are presented in Figure 3. Hygroscopic  
19 water content has been shown to strongly correlate ( $r^2 > 0.9$ ) with soil clay content (Petersen et  
20 al., 1996) and even though this relationship has some mineralogy dependence it still provides a  
21 good, low-cost, surrogate for soil clay percentage. The hygroscopic water content for a 2:1 Ca  
22 saturated montmorillonite, such as that present on this field site, is  $0.19 \text{ g g}^{-1}$  at a relative  
23 humidity of 50%. Which means soil clay percentage in the fine earth fraction ( $<2\text{mm}$ ) is likely to  
24 vary from no clay to values of up to  $\sim 44\%$  across the catchment, which is consistent with the  
25 hand texturing estimates for clays in the upper portion of the catchment and sandy loams in the  
26 lower. In order to identify the contribution of the soil texture to the EMI response, we correlated  
27 the hygroscopic water content with  $EC_a$  values for the different dates and wetting degrees (Table  
28 1); we observed low correlation when the soil was dry and the strongest correlation ( $r^2 \sim 0.5$ )  
29 when the soil was wet. We also analyzed the hygroscopic water content results with the  
30 combined  $EC_a$  response surface, determined using the rank stability of all the data ( $r^2 = 0.5$ ), the  
31 first 3 dry  $EC_a$  response surfaces ( $r^2 = 0.24$ ) and final 3 wet surfaces ( $r^2 = 0.54$ ), again showing

1 the stronger correlation of texture with wet soil. Given the consistency in the correlation, there is  
2 no case for multiple mapping being any better than a single map at field capacity for determining  
3 soil texture, primarily because the critical parameter is water content, as expected, the largest  
4 contrast in electrical response is found approaching saturation.

5 A comprehensive measurement campaign was conducted on February 28<sup>th</sup>, when the  
6 catchment was imaged using EMI and simultaneous point measurements were obtained using a  
7 mobile TDR system. Prior to January the soil had been too hard for routine TDR measurement,  
8 and it wasn't until the soil became softer that the EMI/TDR comparison became feasible; this is  
9 always an issue using insertion measurement techniques such as TDR. We measured volumetric  
10 water content and  $EC_a$  using TDR and at the same time another surveyor measured  $EC_a$  using  
11 EMI; the results are compared in Figure 4. In addition, the  $EC_a$  response surfaces obtained for  
12 both measurement techniques are presented to the right in Fig 4. We observed that the spatial  
13 patterns follow trends with both techniques but TDR  $EC_a$  measurements were about 3 times  
14 lower than the EMI measurements. This is consistent with the different support volumes and the  
15 expectation that the EMI will see more clay (i.e., charged surfaces, ions) because of its greater  
16 penetration into the subsurface, where the clay is expected to increase with depth. This is  
17 supported by vertical  $EC_a$  EMI measurements, which measure deeper into the soil, and indicate  
18 an increase in electrical conductivity with depth.

19 Figure 5 shows three sets of response surfaces, the upper surfaces were determined from  
20 EMI measurements whilst the lower surfaces were determined from TDR measurements. Fig 5A,  
21 shows the VWC estimated from the differencing approach ( $EC_a$  Feb 28<sup>th</sup> –  $EC_a$  Sept 27<sup>th</sup>), whilst  
22 Fig. 5B is the water content estimated directly ( $EC_a$  Feb 28<sup>th</sup>). Parameters used in Equation 1  
23 included a porosity of  $0.57 \pm 0.1$ , and an  $EC_e = 0.1 \text{ S m}^{-1} \pm 0.05$ . The areal average water content  
24 is lower for the differencing approach ( $0.43 \text{ m}^3 \text{ m}^{-3}$ ), and more consistent with the TDR value  
25 ( $0.31 \text{ m}^3 \text{ m}^{-3}$ ) for Fig 5C; however, simulation, used to estimate uncertainty, requires the use of  
26 the original EMI data so that the interpolated differencing approach data cannot be used in the  
27 estimate of uncertainty. The spatial patterns of VWC obtained with the TDR and EMI are similar  
28 with higher values in the upper portion of the catchment (red) and lower values in the lower  
29 portion of the catchment (blue). Results using sequential Gaussian simulation (sGs) show that the  
30 simulated EMI VWC spatial pattern (Fig 5D) corresponds with the interpolated EMI data (Fig  
31 5B); as does the simulated TDR VWC (Fig 5E) with the interpolated TDR data (Fig 5C). sGs is

1 then used to determine the uncertainty in terms of a standard deviation (Fig. 5F and G) and the  
2 signal to noise ratio is determined and presented (SNR: mean over the standard deviation). One  
3 initial observation is the higher structural definition to the patterns from the EMI VWC  
4 compared with TDR VWC, where the sparse TDR data results in similar general patterns but  
5 with lower definition. The TDR data tends to display a graphical ‘bulls-eye’ effect with lower  
6 connectivity in space which is an artifact of the sparse data. Higher VWC values are estimated in  
7 the upper portion of the catchment, however, the EMI data indicate higher VWC in the mid  
8 portion of the catchment also, especially in a couple of linear features running SE to NW,  
9 perpendicular to the stream channel (also identified as zone A in Fig. 8). Investigation of these  
10 zones of higher  $EC_a$  response found that well defined clay bands were running down the slopes  
11 perpendicular to the stream and were buried below ~20 cm of loamy surface soil. Hence, the  
12 smaller support of the TDR measurements didn’t identify these features, while the larger EMI  
13 support volume did. Lower standard deviation was observed for the more exhaustive EMI  
14 measurements in Figure 5F as compared with 5G, which results in a much higher SNR for the  
15 EMI VWC than the TDR VWC in Figures 5H and 5I.

16 Comparison of Figure 5C (TDR) and 5A (diff EMI) and Fig 5C with 5B is shown in the  
17 scatter plot in Figure 6. Direct determination of VWC (Figure 5B) using the EMI data compared  
18 with TDR VWC results in a poor correlation ( $r^2=0.28$ ) and a slope that diverges from a 1:1 line  
19 at low water contents. However, comparison of the TDR data with the differenced EMI (Figure  
20 5A) VWC shows a much stronger correlation  $r^2=0.48$ , and a slope the same as the 1:1 line but  
21 offset to higher water contents (~0.08).

22 Figure 7 presents the VWC estimated from the EMI differencing approach at eight  
23 different times during the period Oct. 2007- Feb. 2008, given that the VWC- $EC_a$  is non-linear,  
24 Fig. 7 is not a simple scaling of the  $EC_a$  response. The patterns, and correlation analysis (Table  
25 1) indicate that moisture and texture are most highly correlated when the soil is wet, but not  
26 when it is dry, which is similar to the finding of Western et al. (2003) who found that moisture  
27 patterns tend to be random when dry and show increasing connectivity and spatial  
28 autocorrelation when wet. The patterns suggest there is reasonable uniformity in VWC across the  
29 catchment up until January, and that this changes to strong, distinct patterns from January  
30 onwards.

1           Figure 8 shows the GPS determined altitude (A), the derived wetness index (Equ.5) (B),  
2 and the EMI diff determined moisture content for February 28<sup>th</sup> (C). The stream path is shown as  
3 the black line on (C), and is consistent with the high values of wetness index on (B). The grey  
4 lines on the moisture content image (C) define areas of overland flow occurring in the catchment  
5 during the associated rainstorm. The black arrows to the wetness index show that these areas are  
6 consistent with zones of convergence in the upper portion of the catchment. Visual comparison  
7 of the wetness index and the VWC suggests that they do not mirror each other; the lack of any  
8 linear correlation between the two data sets confirms this. The convergence zones of the wetness  
9 index are consistent with areas of overland flow and stream flow, however, there are large  
10 proportions of the catchment that have low convergence and high soil moisture. This is  
11 particularly noticeable in zone A for instance, where the increased soil moisture was observed to  
12 occur due to subsurface clay bands, and thus was texture controlled.

13

## 14 **5. Discussion**

15           The use of geophysical techniques in soil science has provided us with a fast and cost-  
16 effective way of collecting large amounts of spatially distributed information. However, the  
17 inversion of geophysical signals into physical parameters requires a good understanding of the  
18 technique as well as knowledge of the soil properties. Often, the combination of different  
19 sensors can contribute to constrain each other and help with parameter estimation. Speed of  
20 measurement, coverage intensity and support volume make EMI well suited to data collection at  
21 this catchment scale. The advantages and disadvantages of determining moisture using  $EC_a$  are  
22 discussed elsewhere. Here, we discuss some of the patterns to emerge from this intensive data  
23 collection.

24           Figure 6, shows the VWC-TDR and VWC-EMI for our catchment, the regression  
25 indicated similar slope but with an offset, so that the EMI recorded higher moisture contents than  
26 the TDR. This result most likely arises due to the instruments having different support volumes,  
27 and raises an intriguing question, “Is the difference in offset simply a calibration artifact, or is it  
28 the result of the sensors responding to moisture in different pore volumes?” A major challenge in  
29 hydrology is to measure and model the impact of macro-pore flow (Zehe et al., 2007; Robinson  
30 et al., 2008a). The clay soil in the upper portion of the catchment was vertic, with large cracks in  
31 the summer. The wetting served to reduce the cracks and reseal much of the surface as fall

1 progressed; however, auger observations during the rainfall events in January indicated that these  
2 cracks had not fully closed below the surface. This created a subsurface intra-ped network of  
3 cracks and flow paths, where the observations revealed subsurface saturated flow at a depth of  
4 ~20cm. This water could be detected by the EMI which would integrate the water in cracks and  
5 large soil blocks, but not by the TDR that mostly explores the soil blocks, given the different  
6 support volumes. It raises a further question of, “what is the appropriate value of porosity for  
7 soils like this?” Porosity, determined from bulk density is normally conducted on samples <1  
8 dm<sup>3</sup>, however, it was clear at the field site that the crack network porosity does not fully seal and  
9 that its contribution becomes important during heavy rain when lateral flows occur and stream  
10 flow is generated. This data is not sufficiently comprehensive, lacking a hydrograph, to tease  
11 apart when the crack network is, or is not, contributing to stream flow, but lateral flows were  
12 only observed at times when stream flow was operational. Though only providing anecdotal  
13 evidence, this data should encourage researchers to test whether electrical measurements, with  
14 different support volumes, can be used to differentiate between water in different pore-networks,  
15 at different scales. More-over, whether geophysical data can be utilized to determine when  
16 macro-pores might be full and active contributing to catchment response.

17 With reference to catchment hydrological processes, the results presented in this work  
18 indicate a transition in moisture behavior between January the 1<sup>st</sup> and 6<sup>th</sup> and support the concept  
19 of preferred soil moisture states as described in Grayson et al. (1997). They state that, “*The wet*  
20 *state is dominated by lateral water movement through both surface and subsurface paths, with*  
21 *catchment terrain leading to organization of wet areas along drainage lines. We denote this as*  
22 *nonlocal control. The dry state is dominated by vertical fluxes, with soil properties and only*  
23 *local terrain (areas of high convergence) influencing spatial patterns. We denote this as local*  
24 *control.*” Prior to January 6<sup>th</sup> there was no stream flow, nor was there any lateral water flow to be  
25 observed from auguring the soil. However, on January the 6<sup>th</sup> after a large rainfall event stream  
26 flow was generated and water was observed to flow laterally in the vertic-soil crack network, as  
27 subsurface flow, in the upper portion of the catchment. Figure 2C indicates a gradual broadening  
28 of the EMI EC<sub>a</sub> histogram that switches between Jan 1<sup>st</sup> and Jan 6<sup>th</sup>. Our interpretation is that this  
29 is consistent with a switch in moisture states from local control to non-local control. The heavy  
30 rain was observed to cause lateral and overland flow, as well as initiating stream flow. Sadly the

1 data set doesn't extend further as it would have been interesting to examine whether there was a  
2 gradual change back in the shape of the histogram, or another sudden switch as the soil dried.

3 With reference to figure 8, our data also support the assertion, that terrain is not the only  
4 control over moisture patterns, and that the moisture patterns (Fig. 8C) do not simply mirror the  
5 wetness index (Fig. 8B). This agrees with the work presented by Wilson et al., (2005) that  
6 showed that prediction of soil moisture in their data sets was poor, based on terrain alone. They  
7 found that incorporation of residual data, which acts as a surrogate for spatially persistent  
8 patterns, potentially related to soil and vegetation type, plus an error term with the terrain data,  
9 gave the best estimate of soil moisture.

10

## 11 **Conclusions**

12 Time-lapse imaging using EMI allowed us to observe soil wetting patterns and moisture  
13 dynamics. Moisture content determination is improved by subtracting the  $EC_a$  response surface  
14 for dry soil from subsequently wetter soil  $EC_a$  response surfaces, and using a model to estimate  
15 moisture content from the  $EC_a$  difference. Differencing in this manner improved correlation  
16 between TDR and EMI water content estimates from  $r^2=0.28$  to  $r^2=0.48$ . Wet  $EC_a$  response  
17 surfaces correlate the best with soil texture, dry images correlate poorly.

18 Data collected using the EMI supports the concept of preferred soil moisture states,  
19 showing a distinct switch in EMI  $EC_a$  response with the initiation of lateral flows and  
20 streamflow. The findings also indicate that the soil moisture patterns do not mirror the catchment  
21 wetness index, though the wetness index does identify zones of convergence where overland  
22 flow occurred, this is in agreement with recent analysis from Australia. In addition, data  
23 indicates that the TDR and EMI, with different support volumes, explore different types of soil  
24 moisture. We conjecture that measuring soil response at specific soil water contents using EM  
25 sensors with different support volumes may allow us to differentiate between the contributions of  
26 the water retained in the matrix from the macro-pore flow.

27

## 28 **Acknowledgements**

29 Thanks to Rosemary Knight, Dept of Geophysics for supporting this research, and to David  
30 Freyberg, Dept of Civil and Env. Engineering, for supplying potential evaporation values for the  
31 area.

1 **References**

2

3 Abdu, H., Robinson, D.A., and Jones, S.B., 2007. Comparing bulk soil electrical conductivity  
4 determination using the DUALEM-1S and EM-38DD EMI instruments. *Soil Sci. Soc. Am. J.* 71,  
5 189–196.

6

7 Abdu H., Robinson, D.A., Seyfried, M. and Jones, S.B., 2008. Geophysical imaging of  
8 watershed subsurface patterns and prediction of soil texture and water holding capacity. *Water*  
9 *Resour. Res.*, 44, W00D18, doi:10.1029/2008WR007043.

10

11 Archie, G.E., 1942. The electrical resistivity log as an aid in determining some reservoir  
12 characteristics. *Trans. Am. Inst. Miner. Metall. Petrol. Eng.* 146, 54–62.

13

14 Barling, R.D., Moore, I.D., Grayson, R.B., 1994. A quasi-dynamic wetness index for  
15 characterizing the spatial distribution of zones of surface saturation and soil water content. *Water*  
16 *Resour. Res.*, 30, (4), 1029-1044. doi:10.1029/93WR03346

17

18 Beven, K.J., 2001. *Rainfall-runoff modeling: The primer*. Wiley, Chichester, UK.

19

20 Beven, K.J., Kirkby, M.J., 1979. A physically based, variable contributing area model of basin  
21 hydrology. *Hydrol Sci Bull* 24 (1), 43–69.

22

23 Besson, A., Cousin, I., Bourennane, H., Nicoullaud, B., Pasquier, C., Richard G., Dorigny, A.,  
24 and King, D., 2010. The spatial and temporal organization of soil water at the field scale as  
25 described by electrical resistivity measurements. *European Journal of Soil Science* 61, 120–132

26

27 Blöschl, G., and R.B., Grayson., 2000. Spatial observations and interpolation. In R.B. Grayson  
28 and G. Blöschl (ed.) *Spatial patterns in hydrology*. p. 17–50. Cambridge Univ. Press, Cambridge,  
29 UK.

30

1 Bogena, H.R., Huisman, J.A., Oberdörster, C., and H. Vereecken., 2007. Evaluation of a low-  
2 cost soil water content sensor for wireless network applications. *Journal of Hydrology* 344, 32-  
3 42.  
4

5 Brabb, E.E., Graymer, R.W., and Jones, D.L., 2000. Geologic map and map database of the Palo  
6 Alto 30' × 60' quadrangle, California. Misc. Field Studies Map MF-2332. U.S. Geol. Surv.,  
7 Reston, VA.  
8

9 Callegary, J.B., Ferre, T.P.A., and Groom, R.W., 2007. Spatial sensitivity of low induction-  
10 number frequency-domain electromagnetic induction instruments. *Vadose Zone J.* 6, 158–167.  
11

12 Cardell-Oliver, Smettem, R.K., Kranz, M., and Mayer, K., 2005. A reactive soil moisture sensor  
13 network: design and field evaluation. *International Journal of Distributed Sensor Networks* 1 (2),  
14 149 – 162.  
15

16 Corwin, D.L., and Lesch, S.M., 2003. Application of soil electrical conductivity to precision  
17 agriculture: Theory, principle, and guidelines. *Agron. J.* 95, 455–471.  
18

19 Dobecki T.L. and Romig, P.R., 1985. Geotechnical and groundwater geophysics. *Geophysics* 50  
20 (I2), 2621 -2636.  
21

22 Doolittle, J.A., Sudduth, K.A., Kitchen, N.R., and Indorante, S.J., 1994. Estimating depths to  
23 claypans using electromagnetic induction methods. *J. Soil Water Conserv.* 49, 572– 575.  
24

25 Dutch S., 2010. Converting UTM to Latitude and Longitude (Or Vice Versa).  
26 <http://www.uwgb.edu/dutchs/UsefulData/UTMFormulas.htm>  
27

28 Engman, E.T., and Chauhan, N., 1995. Status of microwave soil moisture in situ measurements  
29 with remote sensing. *Remote Sen. Environ.* 51, 189-198.  
30

1 Ferré, P.T.A., Knight, J.H., Rudolph, D.L., and Kachanoski, R.G., 1998. The sample areas of  
2 conventional and alternative time domain reflectometry probes. *Water Resour. Res.* 34, 2971–  
3 2979.  
4

5 Freeland, R.S., 1989. Review of soil-moisture sensing using soil electrical-conductivity. *Trans.*  
6 *ASAE* 32, 2190–2194.  
7

8 Friedman, S.P., 2005. Soil properties influencing apparent electrical conductivity: A review.  
9 *Comput. Electron. Agric.* 46, 45–70.  
10

11 Gee, G.W., and T.W., Bauder, 1986. Particle-size analysis. Pages 283-311 in A. Klute, editor.  
12 *Methods of soil analysis*. Second edition. Agronomy Monograph 9, Part 1. Soil Science Society  
13 of America, Madison, Wisconsin, USA.  
14

15 Goovaerts, P., 1997. *Geostatistics for natural resources evaluation*. Oxford Univ. Press, New  
16 York.  
17

18 Goovaerts, P., 1999. Geostatistics in soil sciences: State-of-the-art and perspectives. *Geoderma*,  
19 89, 1–45. doi:10.1016/S0016-7061(98)00078-0.  
20

21 Grayson, R.B., Western, A.W., and Chiew, F.H.S., Blöschl, G., 1997. Preferred states in spatial  
22 soil moisture patterns: Local and nonlocal controls *Water Resour. Res.*, 33 (12), 2897–2908.  
23

24 Grayson, R.B., and Western, A.W., 2001. Terrain and the distribution of soil moisture. *Hydrol*  
25 *Proc.* 15, 2689–2690.  
26

27 Harvey, O.R., and Morgan, C.L.S., 2009. Predicting regional-scale soil variability using a single  
28 calibrated apparent soil electrical conductivity model source. *Soil Sci. Soc. Am. J.* 73 (1), 164-  
29 169.  
30

1 Hendrickx, J.M.H., and R.G., Kachanoski, 2002. Nonintrusive electromagnetic induction. p.  
2 1297–1306. In J.H. Dane and G.C. Topp (ed.) *Methods of soil analysis. Part 4. SSSA Book Ser.*  
3 *5. SSSA, Madison, WI.*  
4

5 Huisman, J.A., Hubbard, S.S., Redman, J.D., and Annan, A.P., 2003. Measuring soil water  
6 content with ground penetrating radar: A review. *Vadose Zone J.* 2, 476–491.  
7

8 Huth, N.I., and Poulton, P.L., 2007. An electromagnetic induction method for monitoring  
9 variation in soil moisture in agroforestry systems. *Australian J. Soil Res.* 45 (1), 63-72.  
10

11 Kachanoski, R.G., and de Jong, E., 1988. Scale dependence and the temporal persistence of  
12 spatial patterns of soil water storage, *Water Resour. Res.*, 24 (1), 85–91.  
13 doi:10.1029/WR024i001p00085.  
14

15 Kirkby, M., 1975. Hydrograph modelling strategies. pp. 69–90, in *Processes in Physical and*  
16 *Human Geography*, edited by R. Peel et al., Heinemann, London.  
17

18 Landon J.R., 1991. *Bookers, tropical soil manual, a handbook for soil survey and agricultural*  
19 *land evaluation in the tropics and subtropics*, Longmans ISBN 0-582-00557-4.  
20

21 Lesch, S.M., Corwin, D.L., and Robinson, D.A., 2005. Apparent soil electrical conductivity  
22 mapping as an agricultural tool for arid zone soil. *Computers and Electronics in Agriculture* 46,  
23 351-378.  
24

25 Lin, H.S., Kogelmann, W., Walker, C., and Bruns M.A., 2006. Soil moisture patterns in a  
26 forested catchment: A hydrogeological perspective. *Geoderma* 131, 345-368.  
27

28 Loague, K., 1992. Soil water content at R-5, 1, Spatial and temporal variability. *J. Hydrol.*, 139,  
29 233–251.  
30

1 McNeill, J.D., 1980. Electromagnetic terrain conductivity measurement at low induction  
2 numbers. Tech Note TN-6. Geonics Ltd., Mississauga, ON, Canada.  
3

4 Michot, D., Benderitter, Y., Dorigny, A., Nicoullaud, B., King, D., and Tabbagh, A., 2003.  
5 Spatial and temporal monitoring of soil water content with an irrigated corn crop cover using  
6 surface electrical resistivity tomography. *Water Resour. Res.* 39, 1138,  
7 doi:10.1029/2002WR001518.  
8

9 Mualem, Y., and Friedman, S.P., 1991. Theoretical prediction of electrical-conductivity in  
10 saturated and unsaturated Soil. *Water Resour. Res.* 27, 2771–2777.  
11

12 Nadler, A., 2005. Methodologies and the practical aspects of the bulk soil EC ( $\sigma_a$ )–soil solution  
13 EC ( $\sigma_w$ ) relations. *Adv. Agron.* 88, 273–312.  
14

15 O'Loughlin, E.M., 1986. Prediction of surface saturation zones in natural catchments by  
16 topographic analysis. *Water Resour. Res.* 22 (5), 794-804.  
17

18 Petersen, L.W., Moldrup, P., Jacobsen, O.H., and Rolston, D.E., 1996. Relations between  
19 specific surface area and soil physical and chemical properties. *Soil Sci.* 161, 9—21.  
20

21 Quinn, P.F., Beven, K.J., and Lamb, R., 1995. "The  $\ln(a/\tan b)$  Index: How to calculate it and  
22 how to use it within the Topmodel Framework," *Hydrological Processes* 9, 161-182.  
23

24 Remy, N., Boucher, A., Wu, J., 2009. *Applied Geostatistics with SGeMS: A User's Guide*  
25 Cambridge University Press, Cambridge, UK.  
26

27 Rhoades, J.D., Manteghi, N.A., Shouse, P.J., and Alves, W.J., 1989. Soil electrical conductivity  
28 and soil salinity: New formulations and calibrations. *Soil Sci. Soc. Am. J.* 53, 433–439.  
29

1 Robinson, D.A., Jones, S.B., Wraith, J.A., Or, D., and Friedman, S.P., 2003. A review of  
2 advances in dielectric and electrical conductivity measurement in soils using time domain  
3 reflectometry. *Vadose Zone J.* 2, 444–475.  
4

5 Robinson, D.A., Campbell, C.S., Hopmans, J.W., Hornbuckle, B.K., Jones, S.B., Knight, R.,  
6 Ogden, F., Selker, J., Wendroth, O., 2008a. Soil moisture measurement for ecological and  
7 hydrological watershed scale observatories: A review. *Vadose Zone J.* 7 (1), 358–389.  
8

9 Robinson, D.A., Binley, A., Crook, N., Day-Lewis, F.D., Ferre, T.P.A., Grauch, V.J.S. Knight,  
10 R., Knoll, M., Lakshmi, V., Miller, R., Nyquist, J., Pellerin, L., Singha, K., and Slater, L., 2008b.  
11 Advancing process-based watershed hydrological research using near-surface geophysics: A  
12 vision for, and review of, electrical and magnetic geophysical methods. *Hydrological Processes*  
13 20 (18), 3604-3635.  
14

15 Robinson, D.A., Abdu, H., Jones, S.B., Seyfried, M. Lebron, I., and Knight, R., 2008c. Eco-  
16 geophysical imaging of watershed-scale soil patterns links with plant community spatial patterns.  
17 *Vadose Zone J.* 7 (4), 1132-1138.  
18

19 Robinson, D.A., Lebron, I., Kocar, B., Phan, K., Sampson, M., Crook, N., and Fendorf, S., 2009.  
20 Time-lapse geophysical imaging of soil moisture dynamics in tropical deltaic soils: An aid to  
21 interpreting hydrological and geochemical processes, *Water Resour. Res.* 45, W00D32,  
22 doi:10.1029/2008WR006984.  
23

24 Rodriguez-Iturbe, I., D’Odorico, P., Porporato, A., and Ridolfi, L.. 1999. On the spatial and  
25 temporal links between vegetation, climate, and soil moisture. *Water Resour. Res.* 35, 3709–  
26 3722.  
27

28 Rubin, Y., and Hubbard, S.S., 2006. *Hydrogeophysics*. Springer: New York.  
29

30 Samouelian, A., Cousin, I., Tabbagh, A., Bruand, A., and Richard, G., 2005. Electrical resistivity  
31 survey in soil science: A review. *Soil Tillage Res.* 83, 173–193.

1  
2 Schjonning, P., Thomsen, I.K., Moldrup, P., and Christensen, B.T., 2003. Linking soil microbial  
3 activity to water- and air-phase contents and diffusivities. *Soil Sci. Soc. Am. J.* 67, 156–165.  
4  
5 Schmutge, T.J., and Jackson, T.J., Soil moisture variability, pp. 183–192, in, *Scaling up in*  
6 *hydrology using remote sensing*, edited by J. B. Stewart et al., John Wiley, New York, 1996.  
7  
8 Schwan, J., Fong, H., and Hug, H.K., 1997. Wildfire and oak regeneration at the urban fringe.  
9 *Gen. Tech. Rep. PSW-GTR-160*. U.S. For. Serv., Pac. Southw. For. and Range Exp. Stn.,  
10 Berkeley.  
11  
12 Seneviratne, S.I., Corti, T., Davin, E.L., Hirschi, M., Jaeger, E.B., Lehner, I., Orlowsky, B., and  
13 Teuling, A.J., 2010. Investigating soil moisture-climate interactions in a changing climate: A  
14 review. *Earth-Science Reviews* 99 (3-4), 125-161. doi:10.1016/j.earscirev.2010.02.004.  
15  
16 Sheets, K., and Hendrickx, J., 1995. Noninvasive soil water content measurement using  
17 electromagnetic induction, *Water Resour. Res.* 31 (10), 2401– 2409. doi:10.1029/95WR01949.  
18  
19 Sherlock, M., and McDonnell, J.J., 2003. A new tool for hillslope hydrologists: Spatially  
20 distributed measurements of groundwater and soil water using electromagnetic induction,  
21 *Hydrol. Processes* 17 (10), 1965– 1978. doi:10.1002/hyp.1221.  
22  
23 Stephenson, G.A., and Freeze, R.A., 1974. Mathematical simulation of subsurface contributions  
24 to snowmelt and runoff, Reynolds Creek watershed, Idaho, *Water Resour. Res.* 10, 284–294.  
25  
26 Sudduth K.A., Drummond, S.T., Kitchen, N.R., 2001. Accuracy issues in electromagnetic  
27 induction sensing of soil electrical conductivity for precision agriculture. *Computers and*  
28 *Electronics in Agriculture* 31, 239–264.  
29  
30 Telford, W.M., Geldart, L.P., and Sheriff, R.E., 1990. *Applied Geophysics*. 2nd ed. Cambridge  
31 Univ. Press, New York.

1  
2 Topp, G.C., Davis, J.L., and Annan, A.P., 1980. Electromagnetic determination of soil-water  
3 content- measurements in coaxial transmission-lines. *Water Resour. Res.* 16, 574–582.  
4  
5 Triantafilis, J., and Lesch, S.M., 2005. Mapping clay content variation using electromagnetic  
6 induction techniques, *Comput. Electron. Agric.* 46 (1–3), 203–237.  
7 doi:10.1016/j.compag.2004.11.006.  
8  
9 Tromp-van Meerveld, H.J., and McDonnell, J.J., 2009. Assessment of multi-frequency  
10 electromagnetic induction for determining soil moisture patterns at the hillslope scale, *J Hydrol.*  
11 368 (1-4), 56-67.  
12  
13 Vachaud, G., Passerat de Silans, A., Balabanis, P., and Vauclin. M., 1985. Temporal stability of  
14 spatially measured soil water probability density function. *Soil Sci. Soc. Am. J.* 49, 822–828.  
15  
16 Vereecken, H., Huisman, J.A., Bogaen, H., Vanderborght, J., Vrugt, J.A., Hopmans, J.W., 2008.  
17 On the value of soil moisture measurements in vadose zone hydrology: A review. *Water Resour.*  
18 *Res.* 44, W00D06, doi:10.1029/2008WR006829.  
19  
20 Vitharana, U.W.A., Van Meirvenne, M., Simpson, D., Cockx, L., De Baerdemaeker, J., 2008.  
21 Key soil and topographic properties to delineate potential management classes for precision  
22 agriculture in the European loess area. *Geoderma* 143 (1-2), 206-215.  
23  
24 Western, A.W. and Grayson, R.B., 1998. The Tarrawarra data set: Soil moisture patterns, soil  
25 characteristics, and hydrological flux measurements. *Water Resour. Res.* 34(10), 2765–2768.  
26  
27 Western, A.W., Grayson, R.B., Blöschl, G., Willgoose, G.R., and McMahon, T.A., 1999.  
28 Observed spatial organization of soil moisture and its relation to terrain indices. *Water Resour.*  
29 *Res.* 35 (3), 797–810.  
30

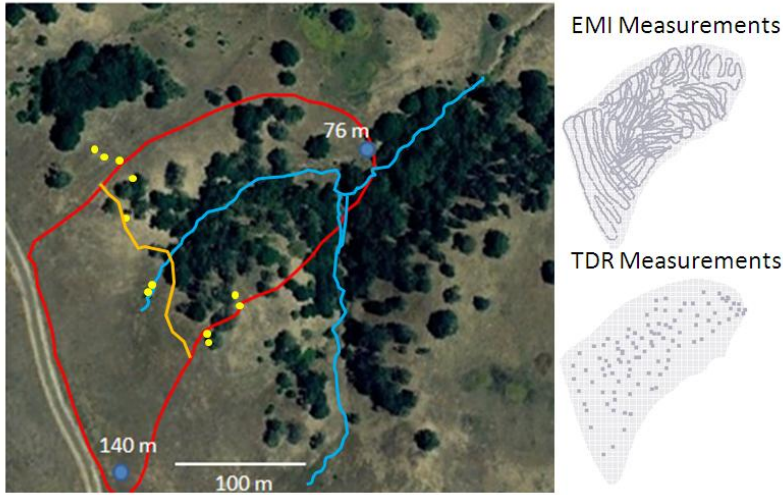
1 Western, A.W., Grayson, R.B., and Blöschl, G., 2002. Scaling of soil moisture: A hydrologic  
2 perspective. *Annu. Rev. Earth Planet. Sci.* 30, 149–180.  
3  
4 Western, A.W., Zhou, S.L., Grayson, R.B., McMahon, T.A., Blöschl, G., Wilson, D.J., 2003.  
5 Spatial correlation of soil moisture in small catchments and its relationship to dominant spatial  
6 hydrological processes. *J. Hydrol.* 286 (1–4), 113–34.  
7  
8 Williams, R.E., 1988. Comment on “Statistical theory of groundwater flow and transport: Pore to  
9 laboratory, laboratory to formation, and formation to regional scale” by Gedeon Dagan, *Water*  
10 *Resour. Res.* 24, 1197–1200.  
11  
12 Wilson David J. \*, Andrew W. Western, Rodger B. Grayson 2005 A terrain and data-based  
13 method for generating the spatial distribution of soil moisture *Advances in Water Resources* 28  
14 (2005) 43–54  
15  
16 Wraith, J.M., Robinson D.A., Jones S.B. and Long D.S., 2005. Spatially characterizing bulk  
17 electrical conductivity and water content of surface soils with time domain reflectometry,  
18 *Computers and Electronics in Agriculture* 46, 239-261.  
19  
20 Zebroski, O., and McBride, J., 1983. *Vegetation management plan*. Stanford Univ. Planning  
21 Office, Stanford, CA.  
22  
23 Zehe, E., Elsenbeer, H., Lindenmaier, F., Schulz, K., and Blöschl, G., 2007. Patterns of  
24 predictability in hydrological threshold systems. *Water Resour. Res.* 43 (7), W07434,  
25 doi:10.1029/2006WR005589.  
26

1  
2

	Sept 27	Oct 4	Oct 22	Nov 11	Dec 5	Jan 1	Jan 6	Jan 10	28 Feb
Sept 27	1.00								
Oct 4	0.71	1.00							
Oct 22	0.76	0.73	1.00						
Nov 11	0.75	0.67	0.84	1.00					
Dec 5	0.76	0.71	0.87	0.85	1.00				
Jan 1	0.64	0.53	0.79	0.83	0.83	1.00			
Jan 6	0.52	0.43	0.68	0.71	0.70	0.87	1.00		
Jan 10	0.51	0.43	0.67	0.71	0.71	0.87	0.96	1.00	
Feb 28	0.57	0.47	0.71	0.72	0.73	0.85	0.93	0.92	1.00
Hygro	0.23	0.12	0.27	0.40	0.34	0.54	0.54	0.56	0.49

3 Table 1. Correlation ( $r^2$ ) between EMI determined water content response surfaces. Hygro is the  
4 hygroscopic water content  $\text{g H}_2\text{O g}^{-1}$  dry soil.

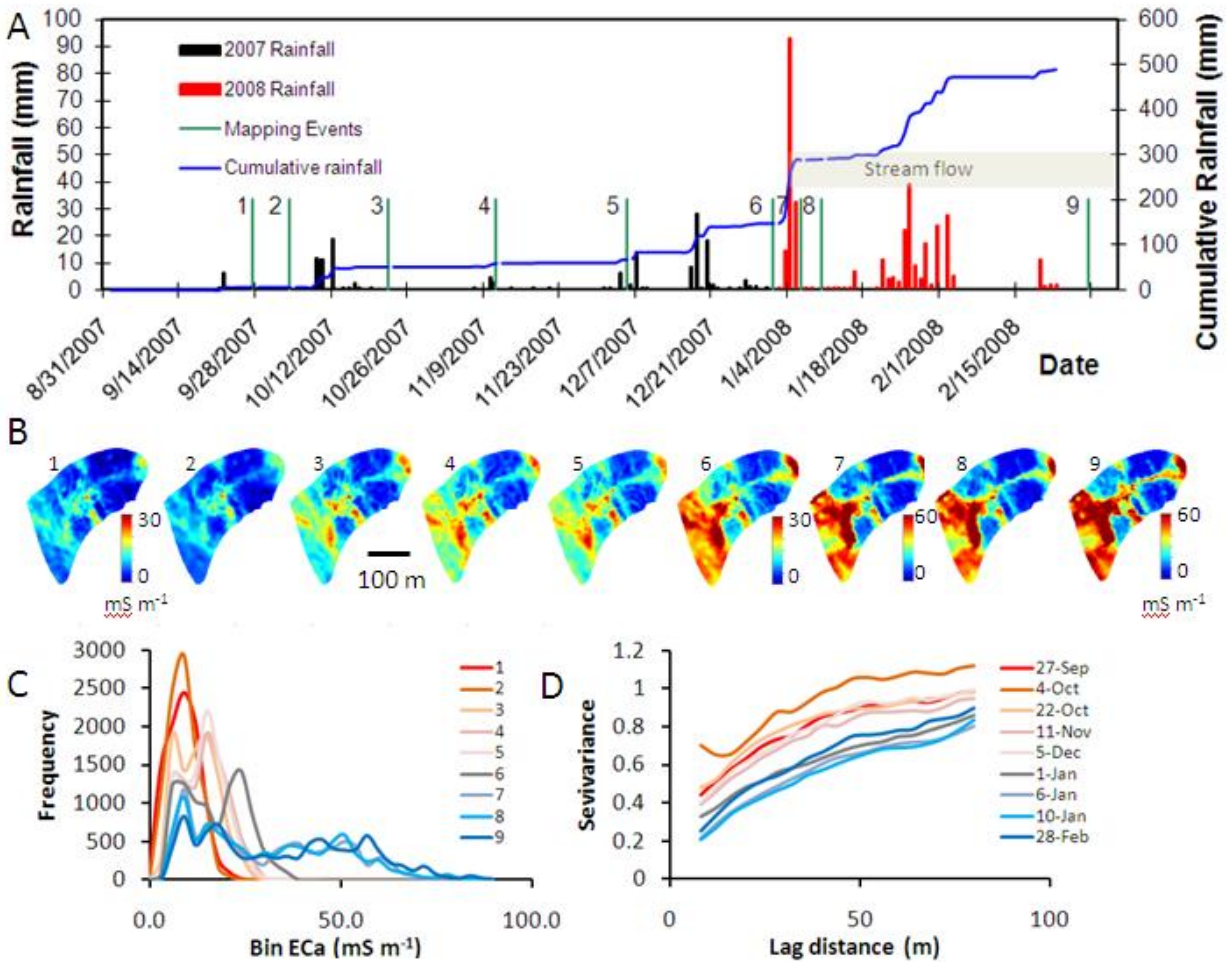
5  
6  
7  
8  
9  
10



1  
2  
3  
4  
5  
6  
7  
8

Figure 1. Four ha catchment in the Stanford foothills reserve, CA. The red line indicates the catchment boundary, the orange line demarks the change from basalt rock to sandstone, and the yellow dots are sandstone outcrops. Stream channels are represented in blue. At right are the EMI measurement tracks and TDR probe insertion locations from Feb 28, 2008.

1



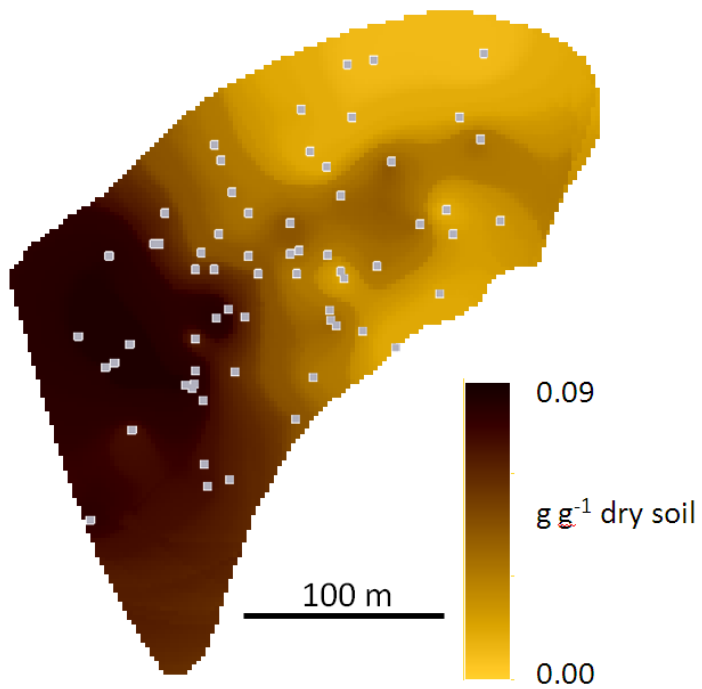
2

3 Figure 2. A) Rainfall between September 2007 and March 2008. B) kriged EMI EC<sub>a</sub> maps  
4 corresponding to green lines with dates numbered on graph A (Note change of scale for 7,8 and  
5 9), C) EC<sub>a</sub> histograms , 1-9 refer to the dates in figure D, and D) corresponding semi-variograms  
6 for each mapping date shown.

7

8

1

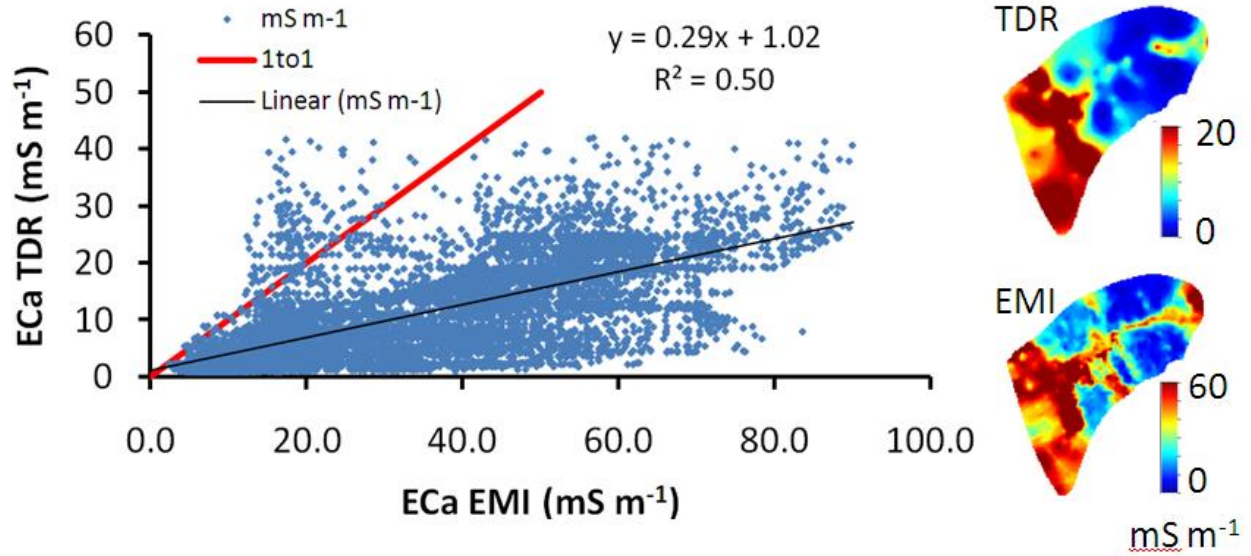


2

3 Figure 3. Hygroscopic water content of the top 20 cm of soil determined from 64 soil samples  
4 collected using a random sampling (squares); the highest value was 0.84 g H<sub>2</sub>O g<sup>-1</sup> dry soil. The  
5 dark areas represent clay in the fine earth fraction (< 2 mm), whereas, the pale colors represent  
6 sand in the fine earth fraction.

7

1



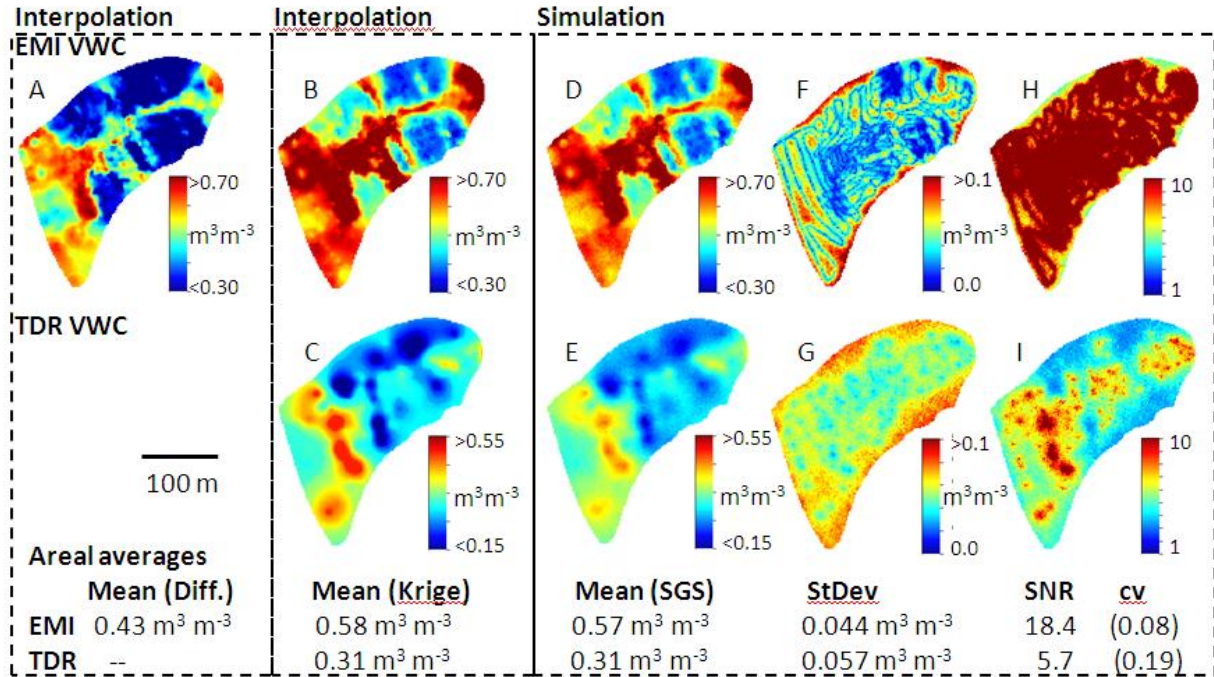
2

3 Figure 4. Comparison of spatially correlated EC<sub>a</sub> determinations made with TDR and with EMI.

4 The EMI readings are approximately three times larger, possibly due to the larger, deeper  
5 sampling volume of the EMI compared to the 10 cm sampling depth of the TDR.

6

1

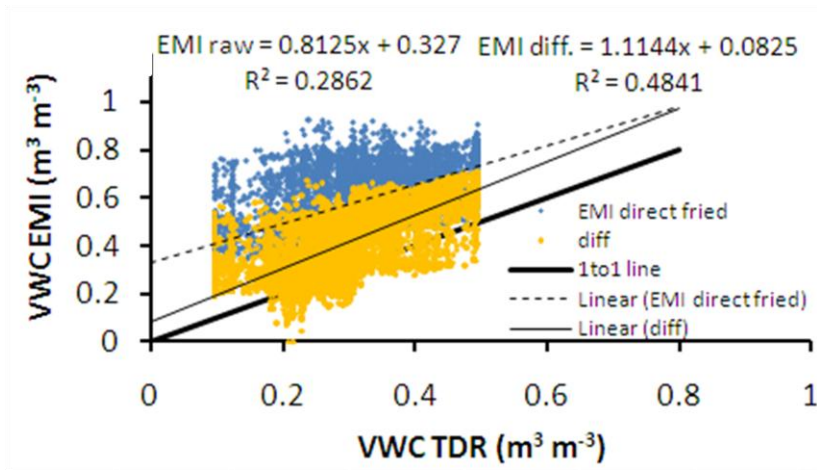


2

3 Figure 5. Response surfaces for, volumetric water content (VWC) determined with EMI (top  
 4 row) and TDR (bottom row). 5A is the VWC estimated from the EMI EC<sub>a</sub> value after  
 5 differencing (EC<sub>a</sub> Feb 28<sup>th</sup> – EC<sub>a</sub> Sept 27<sup>th</sup>). Fig 5B uses the raw EMI EC<sub>a</sub> data to determine  
 6 VWC, whilst Fig 5C is VWC determined using the TDR. Fig 5D and E is the VWC determined  
 7 using simulation, whilst Fig 5F and G is the standard deviation determined from simulation. The  
 8 signal to noise ratio (SNR), Fig 5H and I, is the mean over the standard deviation (strong signal  
 9 for values >1).

10

1

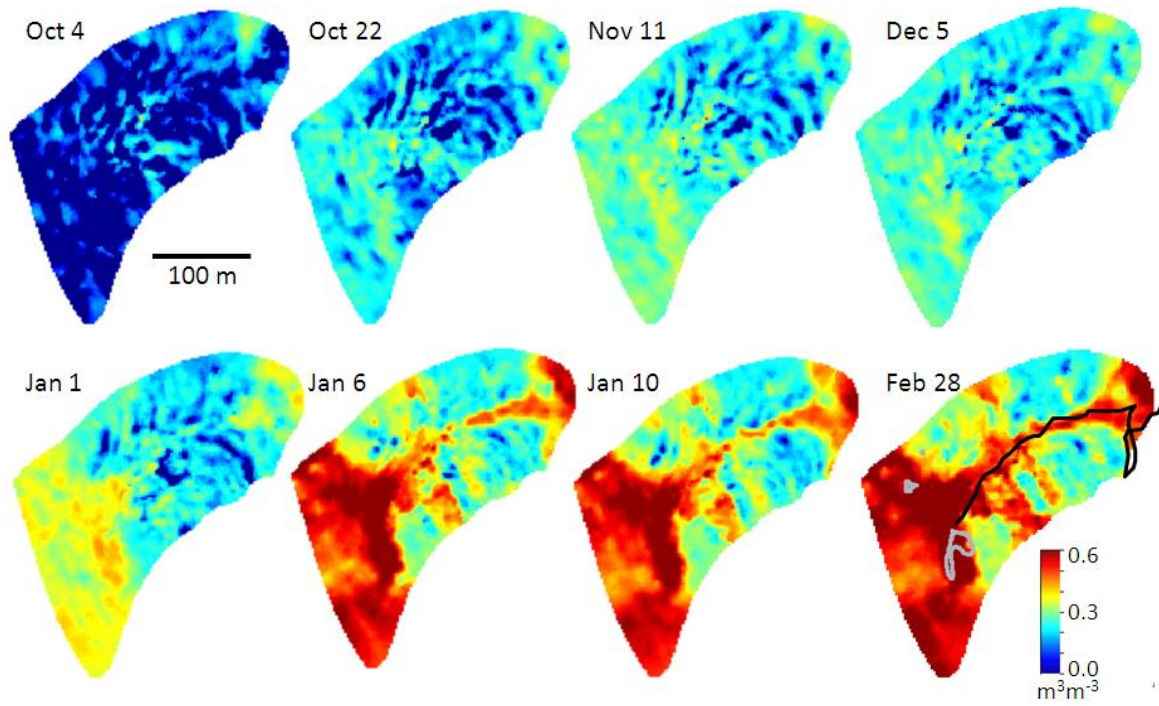


2

3 Figure 6. Comparison of volumetric water content (VWC) determined from i) EMI using direct  
4 estimation from raw data (EMI raw) and from ii) the differencing approach (EMI diff).

5

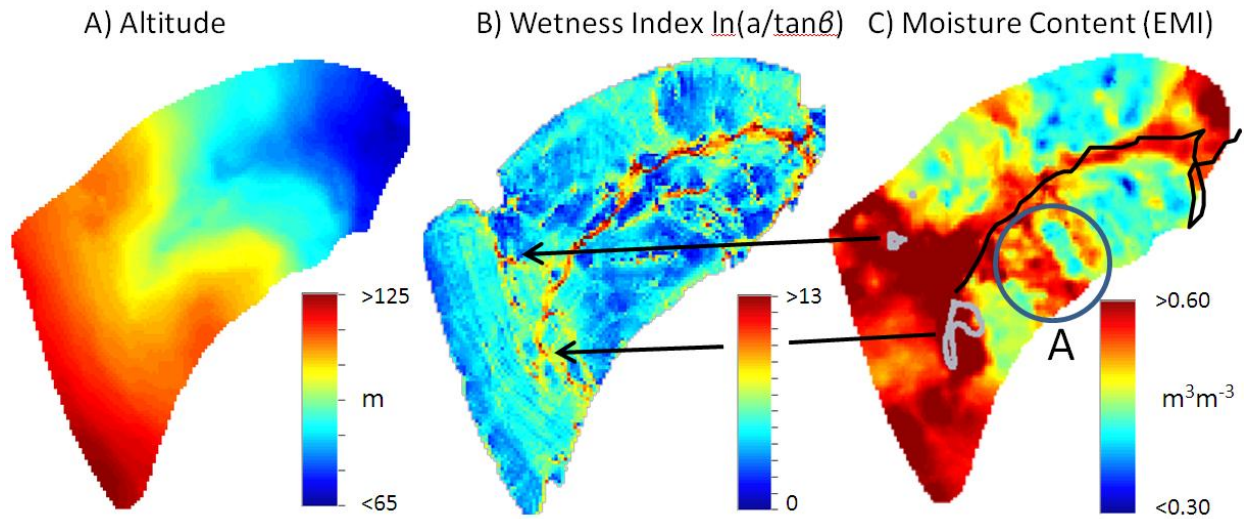
1



2

3 Figure 7. Evolution of volumetric water content (VWC) pattern estimates using the EMI  
4 differencing approach on eight different days during 2007 and 2008.

5



1  
 2 Figure 8. Altitude derived from GPS data, wetness index based on the altitude data, and moisture  
 3 content determined using the differencing approach for Feb 28<sup>th</sup>. The red and yellow points in the  
 4 wetness index denote locations of topographic convergence. The black line on the soil moisture  
 5 image is the stream channel and the grey lines mark the boundary of observed overland flow  
 6 during this event. The arrows indicate the correspondence between the location of the overland  
 7 flow and the convergence zones determined by the wetness index.

8  
 9